1992

Effects of Wind, Density, and Bathymetry on a One-Layer Southern Ocean Model

John M. Klinck
Old Dominion University, jklinck@odu.edu

Original Publication Citation

Klinck, J. M. (1992). Effects of wind, density, and bathymetry on a one-layer Southern Ocean model. *Journal of Geophysical Research-Oceans, 97*(C12), 20179-20189. doi: 10.1029/92jc02058

JOURNAL OF GEOPHYSICAL RESEARCH, VOL. 97, NO. C12, PAGES 20,179–20,189, DECEMBER 15, 1992

Effects of Wind, Density, and Bathymetry on a One-Layer Southern Ocean Model

JOHN M. KLINCK

Department of Oceanography, Old Dominion University, Norfolk, Virginia

Steady solutions from a one-layer, wind-driven, primitive equation model are analyzed to determine the importance of wind forcing, pressure gradient force due to the climatological density distribution and bottom form drag on circulation in the Southern Ocean. Five simulations are discussed: three wind-forced simulations with differing bathymetry (flat bottom, 15% bathymetry, and full bathymetry), one case with full bathymetry forced with the density-induced pressure force, and one case with full bathymetry forced by both wind and density-induced pressure gradients. The simulations presented here confirm the previous speculation (Munk and Palmén, 1951) that form drag is effective in balancing the driving force due to the surface wind stress. In fact, it has such a strong effect that bathymetry with only 15% of the true amplitude reduces the transport from over 480×10^6 m^3 s^{-1} to about 190×10^6 m^3 s^{-1}. If the true bathymetry is used, the total transport is reduced to a value around 20×10^6 m^3 s^{-1}. Analysis of the zonally integrated momentum in the unblocked latitudes of the Southern Ocean shows that the bottom form drag balances the surface forcing, even for simulations that have viscosities that are in the upper range of acceptable values. The vertically integrated pressure gradient due to the climatological density distribution produces a body force that accelerates the Antarctic Circumpolar Current, producing a transport of about 250×10^6 m^3 s^{-1}. Therefore the pressure gradient produced by the density structure of the Southern Ocean is an integral part of the dynamics of the Antarctic Circumpolar Current. It forces the flow across bathymetry that would, in the absence of the spatially varying density field, block the circulation. This result is in contrast to mid-latitude gyres in which the steady, wind-driven circulation is insulated from the influence of bathymetry by stratification (Anderson and Killworth, 1977).

1. INTRODUCTION

During the past 15–20 years, much effort has been focused on understanding the circulation of the Antarctic Circumpolar Current (ACC). However, the momentum balance that produces the observed circulation of the ACC is still not well known. A variety of processes have been suggested [*Nowlin and Klinck*, 1986; *Johnson and Bryden*, 1989; *Wolff et al.*, 1991] to balance the momentum input through wind stress, which is the primary motive force for this current.

The most obvious mechanism to balance wind stress is bottom form drag, which was proposed by *Munk and Palmén* [1951]. However, in vertically averaged models with uniform density, form drag is too effective in removing momentum, which is apparent from the strong reduction in the integrated volume transport in simulations with variable bottom topography [*Bryan and Cox*, 1972; *Schulman*, 1975]. The inclusion of stratification in a flat bottom model produces a volume transport that is too large [*Gill and Bryan*, 1971], relative to an annual mean transport at Drake Passage of 125×10^6 m^3 s^{-1} [*Whitworth and Peterson*, 1985]. Even the introduction of bathymetry in the form of a wall in Drake Passage that blocks two-thirds of the channel results in transport values that are too high. Recent World Ocean circulation models [e.g., *Semtner and Chervin*, 1988] with realistic bathymetry and stratification generate transport of the ACC that is high by almost a factor of 2. The most realistic model of the Southern Ocean, the Fine Resolution Antarctic Model (FRAM) project in England, produces a transport of about 190×10^6 m^3 s^{-1} after 5500 days of simulation (*FRAM News*, no. 3, November 1990). However, the volume transport of the Antarctic Circumpolar Current is declining toward the end of the simulation, which may be a response to modifications in the dynamical processes and parameters in the model.

A second mechanism for balancing the wind stress is divergence of momentum fluxes due to mesoscale eddies. The interaction of eddies and bottom topography and its effect on the dynamics of the ACC has been considered in a recent study [*Wolff et al.*, 1991], which extends the work of *McWilliams et al.* [1978] by considering the effect of bathymetry on a two-layer, quasi-geostrophic, eddy-resolving channel model. Bathymetry is found to be effective in opposing the wind stress, and bottom friction (linear loss in the lower layer) is of secondary importance except along latitude lines that do not cross bathymetry, i.e., along latitudes where the depth is uniform. Lateral friction is a negligible factor in the dynamical balance because of the choice of biharmonic representation for subgrid-scale friction and because there is no stress on the lateral walls. Form drag due to the bathymetry of Macquarie Ridge (even when it is diminished in size because of the quasi-geostrophic constraint) is shown to be the most important mechanism for momentum loss [*Wolff et al.*, 1991, Figure 19].

The purpose of this modeling study is to consider the effects of wind, bathymetry, and density gradients on the circulation of the Southern Ocean. Of particular interest is the momentum balance in the zonal part of this ocean, where the traditional dynamical balance for subtropical gyres is not appropriate. The dynamical balance for this part of the ACC is investigated by calculating the terms in the zonally averaged eastward momentum balance from the steady, forced circulation.

Two external forces are considered: surface stress due to the wind and pressure gradients due to internal density

Paper number 92JC02058.
0148-0227/92/92JC-02058$05.00

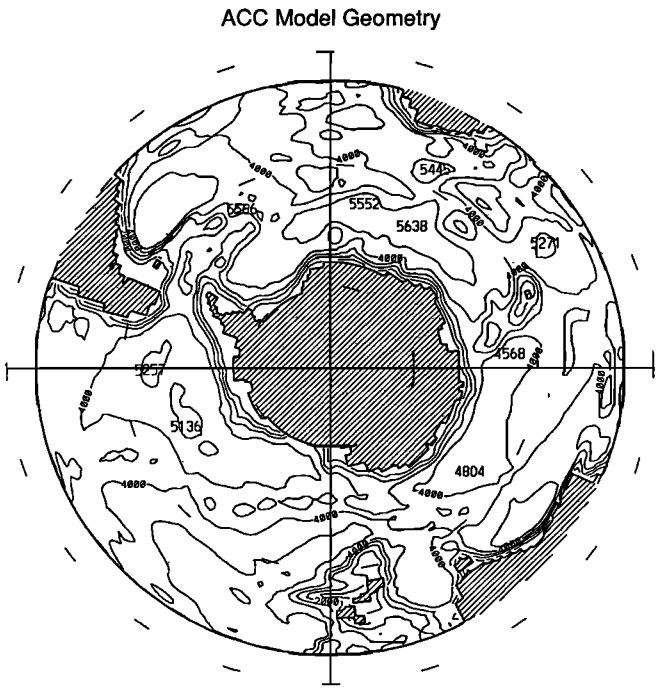

Fig. 1. Geometry and bathymetry of the Southern Ocean as represented in the model. Heavy lines are continental boundaries, while lighter lines are isobaths with an interval of 1000 m. Numbers on the figure indicate depth in meters of isolated high and low spots. Continental land masses are shaded.

variations. The circulation obtained from the model forced by the internal pressure gradients is essentially a diagnostic calculation with viscous drag. It is more appropriate to specify the initial distribution of density and allow the circulation to adjust to a geostrophic balance. However, this calculation requires a fully three-dimensional dynamical model and considerable computer time. In fact, the three-dimensional calculation, among others, has been pursued by the FRAM project in England (for more information, see *FRAM News*, published by Institute of Oceanographic Sciences, Wormley). One result of the present study is that it is possible to include the effects of internal density distributions without having to make a fully three-dimensional calculation.

The remainder of the paper is organized as follows. Section 2 describes the numerical circulation model. Section 3 discusses five cases that are used to analyze the dynamical balances calculated from the steady state circulation. Section 4 considers the zonally integrated momentum balance for these cases. The last section is a summary.

2. Model Formulation

Model Geometry

The domain of interest for this calculation extends from the Antarctic continent to the northern side of the southern subtropical gyres, encompassing the region from 75°S to 25°S (Figure 1). The domain extends far enough north to include most of the subtropical gyres, thus insulating the ACC from the influence of the northern model boundary and allowing the location of the ACC to be determined by the wind forcing and bathymetry rather than by an artificial constraint imposed by the model boundaries.

The resolution for the finite difference circulation model is 1° longitude by 0.5° latitude. Bathymetry, at this resolution (Figure 1), is extracted from 5′ × 5′ bathymetry (from National Geophysical Data Center in Boulder, Colorado); the zero depth contour from this bathymetry data set defines the continental boundaries appropriate for this grid resolution. The bathymetry is smoothed by two passes of a five-point smoother in order to avoid single-point bathymetric features and to ensure that the resolution of the bathymetry matches that of the model.

Surface Wind Stress

The climatological wind stress, prepared by *Trenberth et al.* [1989] from surface forecasts produced by the European Centre for Medium-Range Weather Forecasting, is used to force the circulation. The annual mean wind stress, originally on a 2.5° × 2.5° grid, is interpolated to the 1° × 0.5° model grid (Figures 2*a* and 2*b*). The wind stress is mainly eastward because of the mid-latitude westerlies over the Southern Ocean. The strongest eastward stress occurs in the Indian Sector of the Southern Ocean with a magnitude reaching 0.3 N m^{-2}.

Model Equations and Numerical Procedure

The governing equations for this model are the vertically averaged primitive equations with a free surface in a periodic, β-plane, zonal channel. The primitive equations are used rather than those based on the quasi-geostrophic assumption to allow inclusion of the fully bathymetry in the simulations. The governing equations for the horizontal velocity components (u, v) (eastward and northward, respectively) and the surface elevation (η) are

$$\frac{D}{Dt}u = +fv - g\frac{\partial \eta}{\partial x} - ru + A\nabla^2 u + \frac{\tau^x}{\rho_0 h} \tag{1}$$

$$\frac{D}{Dt}v = -fu - g\frac{\partial \eta}{\partial y} - rv + A\nabla^2 v + \frac{\tau^y}{\rho_0 h} \tag{2}$$

$$\frac{\partial \eta}{\partial t} = -\frac{\partial (hu)}{\partial x} - \frac{\partial (hv)}{\partial y} \tag{3}$$

$$\frac{D}{Dt} = \frac{\partial}{\partial t} + u\frac{\partial}{\partial x} + v\frac{\partial}{\partial y}$$

where $h(x, y) = H - \eta_b(x, y)$ is the time independent local water thickness, H is the area mean depth over the entire model domain, $\eta_b(x, y)$ is the departure of the local depth from the area mean value. The Coriolis parameter varies with latitude ($f = f_0 + \beta y$) as appropriate for the β plane representation of a spherical Earth. The remaining parameters in the model are gravity g, a reference density ρ_0, linear friction r, and lateral friction A. The linear loss term represents a number of drag forces including bottom friction, wave drag, or other processes that tend to retard the geostrophic flow [*Clarke*, 1982]. For the purposes of this study, these processes are referred to collectively as bottom friction, which in a general sense they are.

The time dependent model equations are solved with an

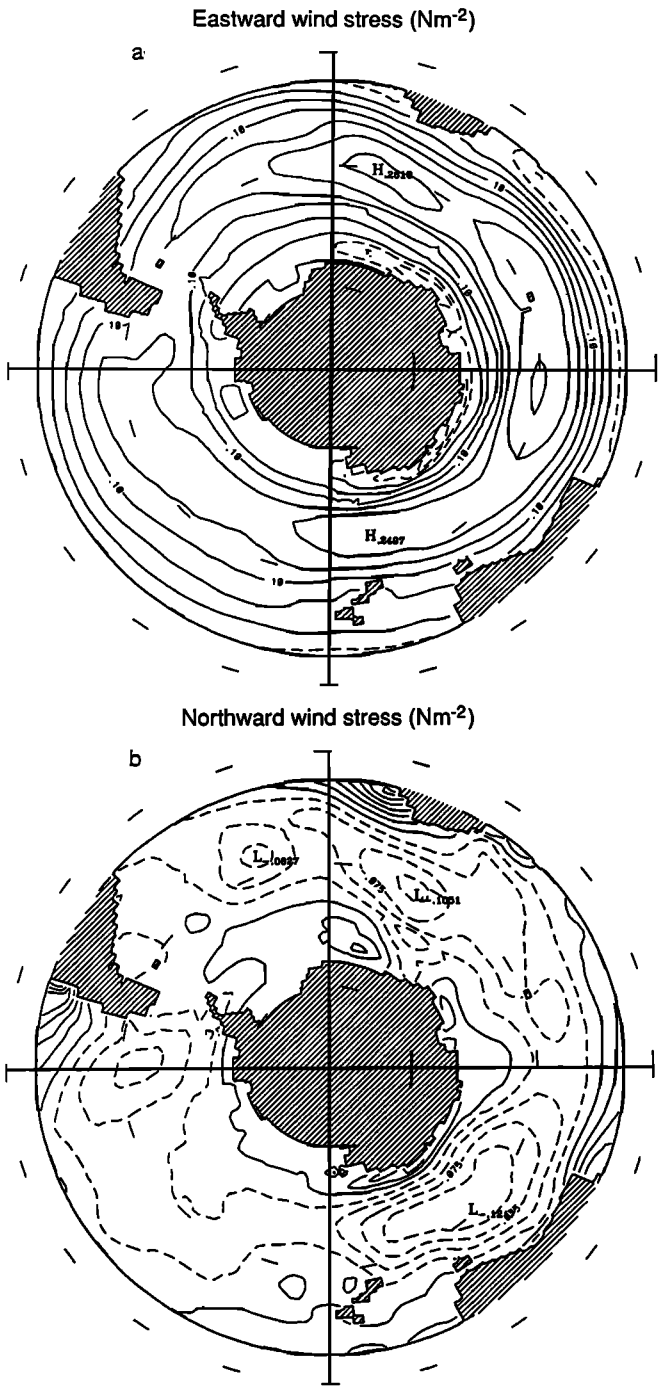

Fig. 2. Annual mean wind stress (N m^{-2}) from *Trenberth et al.* [1989]. Dashed lines indicate negative values. (*a*) Eastward wind stress component (contour interval is 0.05 N m^{-2}). (*b*) Northward wind stress component (contour interval is 0.025 N m^{-2}).

alternating direction implicit (ADI) scheme [*Leendertse*, 1967] on a spatially staggered C grid [*Mesinger and Arakawa*, 1976]. The ADI method separates the spatial gradients in the governing equations into parts operating separately in the x and y directions. A single model time step of 1 hour is accomplished by two substeps, in which one spatial direction is advanced with an implicit scheme and the other uses an explicit scheme and then vice versa. This split implicit scheme retains the benefit of implicit calculation of the fast gravity waves while requiring the inversion of linear systems of equations with tridiagonal coefficient matrices. Further details of the numerical model are discussed by *Klinck* [1991].

Parameter Choices

All but two of the parameters required for the model can be easily determined. The mean depth (H = 3892 m) is obtained by averaging the depth in the model domain (Figure 1). The central latitude of the β plane is chosen to be 55°S, which determines the values of the Coriolis (f_0) and β parameters as -1.194×10^{-4} s^{-1} and 1.31×10^{-11} m^{-1} s^{-1}, respectively. The gravitational acceleration g is 9.8 m s^{-2}, and the base density ρ_0 is 1000 kg m^{-3}.

The two poorly known parameters in this model are linear damping r and lateral eddy viscosity A. Each of these parameters represents a variety of processes, making estimation of appropriate values difficult. Linear friction represents drag that results from the bottom Ekman layer as well as wave drag and form drag from small-scale (subgrid-scale) bathymetry. *Clarke* [1982] presents a discussion of these processes and suggests values in the range of 10^{-6}–10^{-7} s^{-1} for the Southern Ocean, which result in a spin-down time r^{-1} of 10 to 20 days. The lateral friction parameter is equally difficult to estimate, and values can range from 10^2 to 10^4 m^2 s^{-1} [*Gill*, 1982, p. 518].

The grid spacing constrains the choice of friction parameters, since the thicker of the two possible viscous boundary layers must be resolved. The grid resolution of the model discussed here is approximately 1° of longitude (64 km at 55°S), which gives the minimum values of the linear and lateral friction parameters as 8×10^{-7} s^{-1} and 5×10^3 m^2 s^{-1}, respectively, which are in the upper range of acceptable values. However, the linear spin-down time for this value of bottom friction is about 15 days, which is appropriate for the Southern Ocean. The lateral viscosity is comparable to values used in the large-scale, low-resolution general ocean circulation models [*Bryan and Cox*, 1972]. The simulations considered here use the values 5×10^{-7} s^{-1} and 10^4 m^2 s^{-1} for the linear friction and lateral friction coefficients, respectively. Simulations were attempted with somewhat smaller values for each of these parameters, with the result that the solution developed strong oscillations, as expected if the western boundary layer is not resolved.

Forcing by Density Gradients

The influence of a time invariant, spatially varying density field on the circulation is obtained from a straightforward manipulation of the dynamical equations. The shallow-water equations above (1)–(3) are obtained from the Euler equations, by averaging in the vertical. In the form given above, the density of the water is assumed to be constant, so the pressure gradient force arises only from the slope of the free surface. If the density is not uniform, then a pressure gradient force results from horizontal density variations and two additional terms appear in the governing equations.

The form of these additional terms is obtained as follows. The hydrostatic pressure is

$$p(x, y, z, t) = g\rho_0\eta(x, y, t) + g\int_z^0 \rho(x, y, z)\, dz, \quad (4)$$

where the assumption is made that the spatially varying density is independent of time. If the internal pressure is denoted $\hat{p}$ ($= g \int \rho\, dz$), then the pressure gradient is composed of two parts:

$$-\frac{1}{\rho_0}\nabla p = -g\nabla\eta - \frac{1}{\rho_0}\nabla\hat{p}.$$

This pressure gradient is averaged in the vertical to obtain the additional terms in the governing equation.

The vertical average of some quantity Q is defined as

$$\langle Q\rangle = \frac{1}{h(x, y)}\int_{-h(x, y)}^{0} Q(x, y, z, t)\, dz,$$

and the vertical average of the gradient of any quantity is

$$\langle \nabla Q\rangle = \nabla\langle Q\rangle + \frac{\nabla h}{h}\langle Q\rangle - Q(z = -h)\frac{\nabla h}{h},$$

or more compactly,

$$\langle \nabla Q\rangle = \frac{1}{h}\nabla(h\langle Q\rangle) - Q(z = -h)\frac{\nabla h}{h}.$$

Therefore the vertically averaged pressure gradient with spatially varying density is

$$\left\langle -\frac{1}{\rho_0}\nabla p\right\rangle = -g\nabla\eta - \frac{1}{\rho_0 h}\nabla(h\langle\hat{p}\rangle) + \frac{1}{\rho_0 h}\hat{p}(z = -h)\nabla h. \tag{5}$$

The three terms are the pressure gradient due to a slope of the free surface (which is already present in the shallow-water model), the gradient of the vertically integrated pressure, and the pressure force on the bottom due to the internal density variations. Note that the last two forces have the character in this vertical average of body forces like the wind stress; that is, the term looks like a force per unit area divided by the density and thickness. Thus the strength of the force due to density variations $[-\nabla(h\langle\hat{p}\rangle) + \hat{p}(z = -h)\nabla h]$ can be compared directly with the surface stress.

Estimation of the Force Due to Density Gradients

Gordon and Baker [1986] constructed a temperature, salinity, and density climatology of the Southern Ocean by objectively mapping hydrographic observations onto a regular grid of points (2° longitude by 1° latitude at standard depths). These data were used as described below to estimate the pressure force produced by the internal density gradient (5).

Because of data sparsity, there are locations in the gridded fields, usually near the bottom or on the continental margin, at which no estimate of temperature or salinity is given. In order to estimate bottom pressure and vertically integrated pressure, it is necessary to integrate through the water column at every ocean point, which requires estimation of the missing values. For this study, missing values were obtained by interpolating the interior temperature and salinity values and then calculating the density rather than trying to interpolate the density directly. Some of the missing values were obtained by horizontal injection, where only one neighbor point was known. In a few places, values needed to be injected vertically into small basins. In all, about 1% of the temperature and salinity points were specified by interpolation or injection.

Once complete temperature and salinity fields are obtained, the density anomaly relative to water at a given depth with a temperature of 0°C and a salinity of 35‰ was calculated. The density anomaly is used in place of the full density in order to remove a large, but dynamically irrelevant, hydrostatic pressure at the bottom, which causes a loss of precision when derivatives are estimated by subtraction. The bottom pressure is calculated by vertically integrating the density anomaly using the trapezoidal rule. The deepest density value is used to calculate the pressure at the bottom, or equivalently, the density anomaly at the bottom is assumed to be the same as that at the deepest standard depth. Once the bottom pressure is calculated, then the vertical integral of the pressure is obtained from the trapezoidal rule.

The vertically averaged pressure and density anomalies, which are obtained by dividing the integrated pressure and the bottom pressure anomalies, respectively, by the local depth (obtained from the same 5′ bathymetry used in the model), are then interpolated onto the surface elevation points on the model grid. This procedure is used so that slight differences in the bathymetry values, which are at different locations and have been smoothed differently, do not cause large errors when derivatives are estimated. The integrated pressure and bottom pressure are recovered from the interpolated values by multiplying by the bathymetry used in the model.

Given the bottom and the integrated pressure, it is straightforward to evaluate (5) for the body force due to the density distribution (Figures 3*a* and 3*b*). The largest values of the forcing range up to 100 N m^{-2}, but most of the values are between 10 and 20 N m^{-2}, which is a factor of 100 larger than the wind stress. In contrast to the wind stress, the density forcing is strongest in the north-south direction, since this is the direction of the largest density change.

3. RESULTS

Five simulations are presented which illustrate the influence of surface wind stress, bathymetry, and pressure gradients due to density variations on the circulation in the Southern Ocean. All other parameters are held fixed in order to compare the influences of these three parts of the calculation. For each simulation, the flow is started from rest and is allowed to adjust until a steady circulation develops. The external forcing is ramped up over 33 days (800 steps) in order to avoid energetic transients; the solutions become steady after about 1.8 years (16,000 steps) of simulation.

The first three simulations are forced by the same surface wind stress but have varying bathymetric heights: a flat bottom, bathymetry with 15% of the true elevation, and the true bathymetry. The fourth simulation uses the full bathymetry but is forced by pressure gradients due to the internal density distribution. The final case combines the wind forcing and the pressure force due to the internal density gradients with the full bathymetry.

Wind-Driven, Flat Bottom Simulation

The first case is an extension of the analytic model of *Hidaka and Tsuchiya* [1953], which used a zonal channel

with a flat bottom. This simulation uses the same basic geometry but includes the continental boundaries of the Southern Ocean. The depth is uniform with H = 3892 m. Forcing is provided by the annual average climatological wind stress.

The most prominent feature of the steady state circulation (Figure 4*a*) is the ACC, which appears as a strong, zonal current in the surface topography which approximates the geostrophic stream function. The total transport through Drake Passage is 483 × 10^6 m^3 s^{-1}. A subtropical gyre which extends around the model domain develops to the north of the ACC. The flow in the southwestern South Atlantic (Figure 4*b*) shows the Falkland (Malvinas) Current, which is incorrectly to the west of the Falkland (Malvinas) Islands. The Brazil Current is present and extends to about 45°S.

Hidaka and Tsuchiya [1953] found that a reasonable choice for lateral friction coefficient resulted in an ACC with a transport of several thousand Sverdrups. The circulation shown in Figure 4 is weaker than their purely zonal case by a factor of about 5, partly because of the somewhat large values of friction coefficients but primarily because of addi-

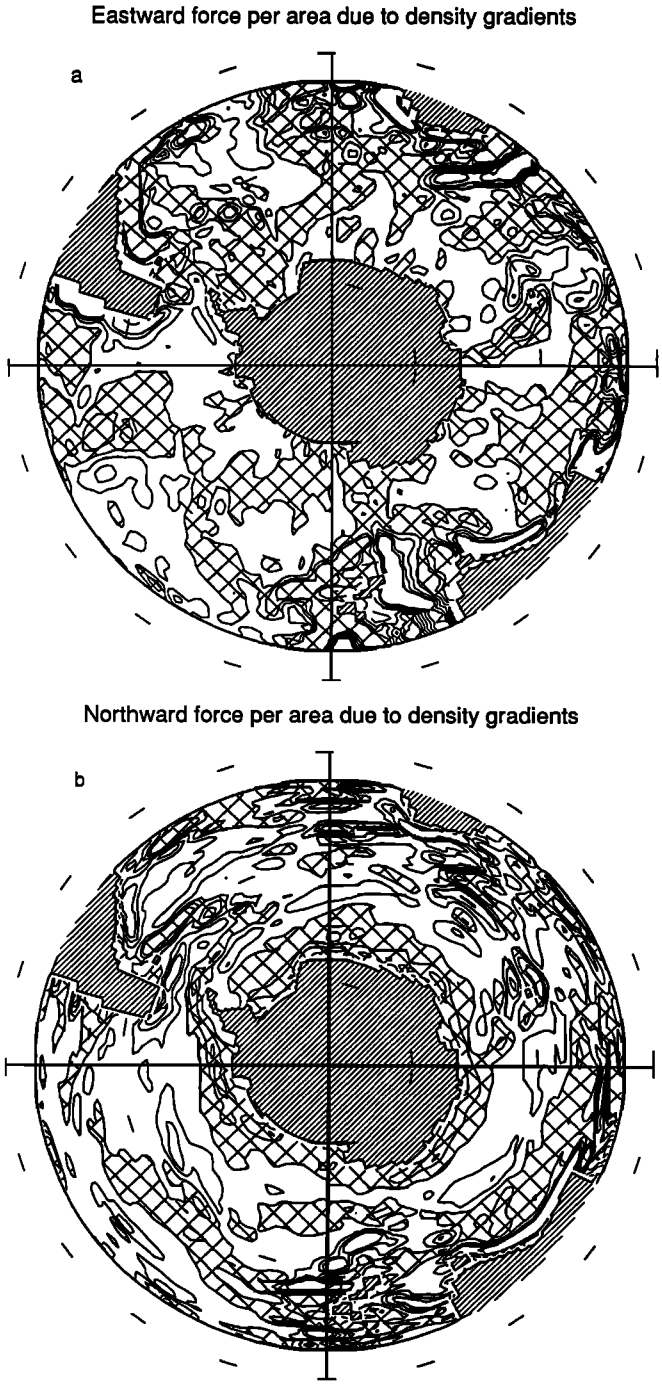

Fig. 3. Body force per unit area (N m^{-2}) due to the distribution of density from the Southern Ocean atlas [*Gordon and Baker*, 1986]. Shaded contours indicate negative values. The contour interval is 20 N m^{-2}. (*a*) Eastward component. (*b*) Northward component.

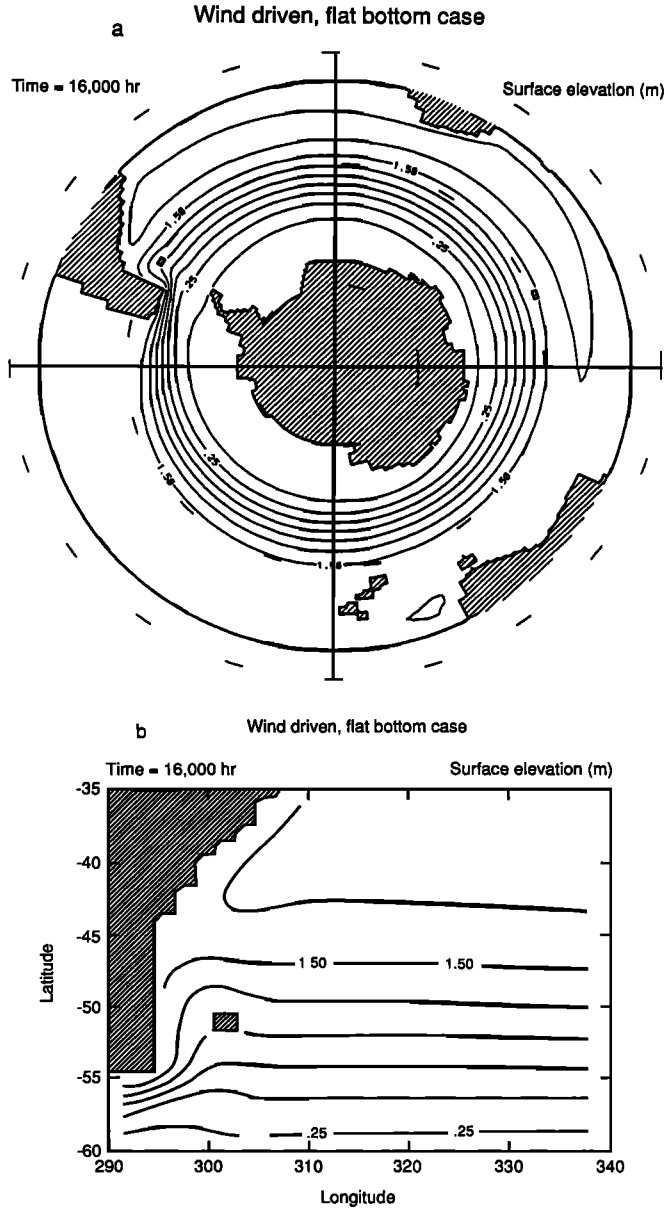

Fig. 4. Surface elevation at steady state for annual mean wind-forced Southern Ocean with a flat bottom. Depth is 3892 m over the whole domain. After 16,000 hours of simulation, the transport is 483 × 10^6 m^3 s^{-1}. The surface topography (in meters) is indicated by thin lines. Heavy lines indicate land boundaries, and land masses are shaded. (*a*) Surface elevation over the whole model domain. Contour interval of 0.25 m. (*b*) Surface topography in the southwestern South Atlantic, with a contour interval of 0.25 m.

tional dissipation at the southern tip of South America due to a viscous western boundary layer. Other simulations (not reported here) with no bottom friction give a steady circulation in the unblocked latitudes between 55°S and 60°S with transports 10 times the value obtained for this case, which is more nearly comparable to the results of *Hidaka and Tsuchiya* [1953].

Wind-Driven, 15% Bathymetry Simulation

The circulation in the previous case is clearly too strong and much too zonal. *Munk and Palmén* [1951] suggested that form drag over a sloping bottom should provide sufficient force to balance the wind. Thus, to simulate this effect, bathymetry was included in the model at 15% of its true amplitude relative to the mean depth. This value of reduction is somewhat arbitrary and was chosen empirically. Simulations with bottom reduction parameters that ranged from 10% to 30% indicated that the most realistic path for the ACC is obtained using a value of 15%.

The steady circulation for this case shows an ACC (Figure 5*a*) with a structure that compares well with the dynamic topography relative to 1400 m (Figure 6) calculated from *Gordon et al.* [1978]. The reference depth is chosen as the zero crossing of the first dynamic mode in Drake Passage [*Inoue*, 1985]. The dynamic topography relative to 1000 or 2500 m (not shown) yields essentially the same pattern.

The strong latitudinal shifts in the simulated flow compare well with similar shifts in the dynamic topography. In particular, there is a southward displacement of the ACC at 30°E, a narrowing of the ACC at 80°E and 160°W, and a northward displacement east of Drake Passage (50°W). However, the total transport in this case (189 × 10^6 m^3 s^{-1}) is a bit larger than the observed value of 125 × 10^6 m^3 s^{-1} [*Whitworth*, 1983]. The total change in surface elevation in the model is about 0.5 m, while the observations give a change of 0.8 dyn m.

The structure of the flow in the southwestern South Atlantic (Figure 5*b*) compares quite well with a schematic description of the flow in this region based on water mass analysis [*Peterson and Whitworth*, 1989, Figure 2]. In the simulated circulation field, the ACC splits near the Falkland Islands, with part continuing to the east as the ACC proper and part going north as the Falkland Current. Offshore of the northward flowing Falkland Current is the southward limb of the Falkland Current and the Brazil Current, which has separated from the South American continent. The recirculation at 310°E, 45°S fits neatly between the Subtropical Front and the Subantarctic Front, as depicted in *Peterson and Whitworth* [1989]. The major difference between the two realizations of the flow is that the simulated Falkland Current flows against the continent, while the observed current flows along the 1000-m isobath, which is farther offshore. This discrepancy results from the strong reduction of bathymetry in the model, which removes the wide continental shelf in this area.

Wind-Driven, Full Bathymetry Simulation

The structure of the steady circulation over the true bathymetry forced by surface wind stress is unrealistic (Figure 7*a*), and the total transport of the ACC is reduced to 20 × 10^6 m^3 s^{-1}. This reduction of the flow by bathymetry

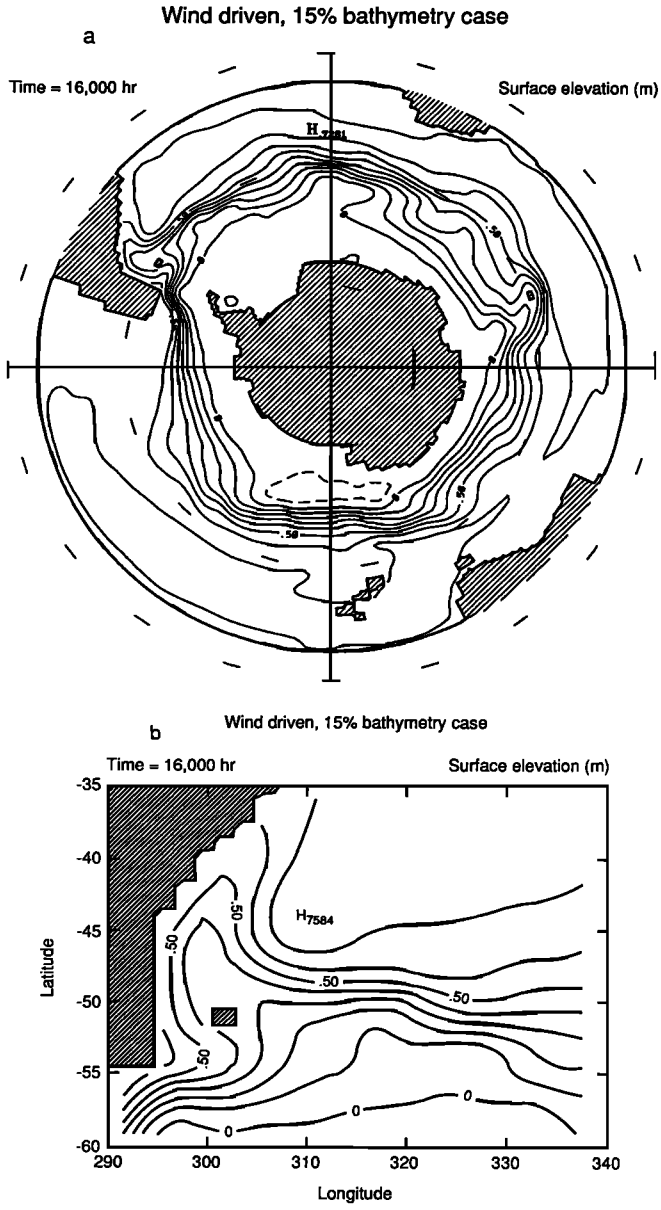

Fig. 5. Surface elevation at steady state for annual mean wind-forced Southern Ocean with bottom topography reduced to 15% of its true value. After 16,000 hours of simulation, the transport is 189 × 10^6 m^3 s^{-1}. Surface elevation (in meters) is indicated by thin lines; negative contour lines are dashed. Heavy lines indicate land boundaries. (*a*) Surface elevation over the whole model domain, with a contour interval of 0.1 m. (*b*) Surface topography in the southwestern South Atlantic, with a contour interval of 0.1 m.

in a one-layer model of the Southern Ocean is not unexpected [*Schulman*, 1975]. The strong topography controls the solution by the requirement that the flow follow isolines of *f*/*h* [*Johnson and Hill*, 1975], thereby resulting in an ACC that follows a convoluted path around the Southern Ocean and extends too far north (e.g., in the South Pacific near 110°W).

The structure of the flow in the southwestern South Atlantic improves in one respect relative to the previous simulation. The Falkland Current (Figure 7*b*) is now east of the Falkland Islands. In other respects though, the circulation is not realistic. In addition to the slow speed, the ACC

extends too far into the Scotia Sea before turning north, the Falkland Current goes too far north before turning southward, and the Brazil Current has been pushed well offshore and extends rather far to the south.

Internal Pressure Gradient Driven, Full Bathymetry Simulation

The steady circulation produced by the pressure force due to internal density gradients has a transport of 256 × 10^6 m^3 s^{-1}. The structure of the circulation (Figure 8*a*) is more realistic (compare to Figure 6) than the previous case, which is driven only by the wind. Two major improvements now arise in the simulated flow field. First, the ACC is deflected less by the bathymetry and follows a more realistic path, compared to the wind-driven, full bathymetry case. Second, the flow speed (transport) is closer to the measured value, although it is still an overestimate by a factor of 2. The unrealistic circulation near the northern side of the model domain is due to the presence of the model boundary. Additionally, the free surface slopes strongly in the vicinity of continental shelves, but such areas are excluded from the dynamic calculation because they are shallower than the reference depth.

The circulation in the southwestern South Atlantic (Figure 8*b*) compares well with the expected circulation. The Falkland Current flows east of the Falkland Islands to about 40°S and returns to about 48°S, where it rejoins the other branch of the ACC. The Brazil Current is evident and penetrates almost to 50°S before flowing north and east to form the poleward limb of the subtropical gyre. However, the simulated ACC penetrates farther into the Scotia Sea than suggested by the schematic flow depicted by *Peterson and Whitworth* [1989, Figure 2].

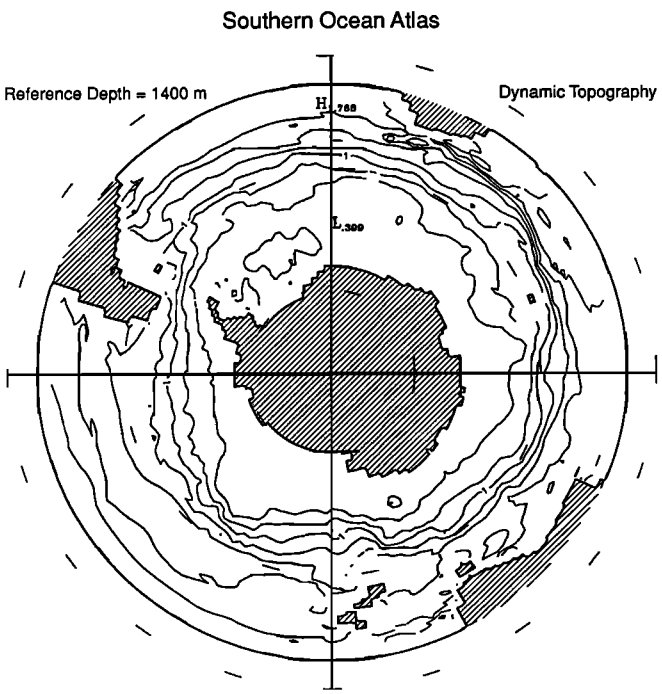

Fig. 6. Dynamic topography (dyn m) of the surface relative to 1400 m calculated from the gridded Southern Ocean atlas data [*Gordon and Baker*, 1986]. Contour interval is 0.2 dyn m.

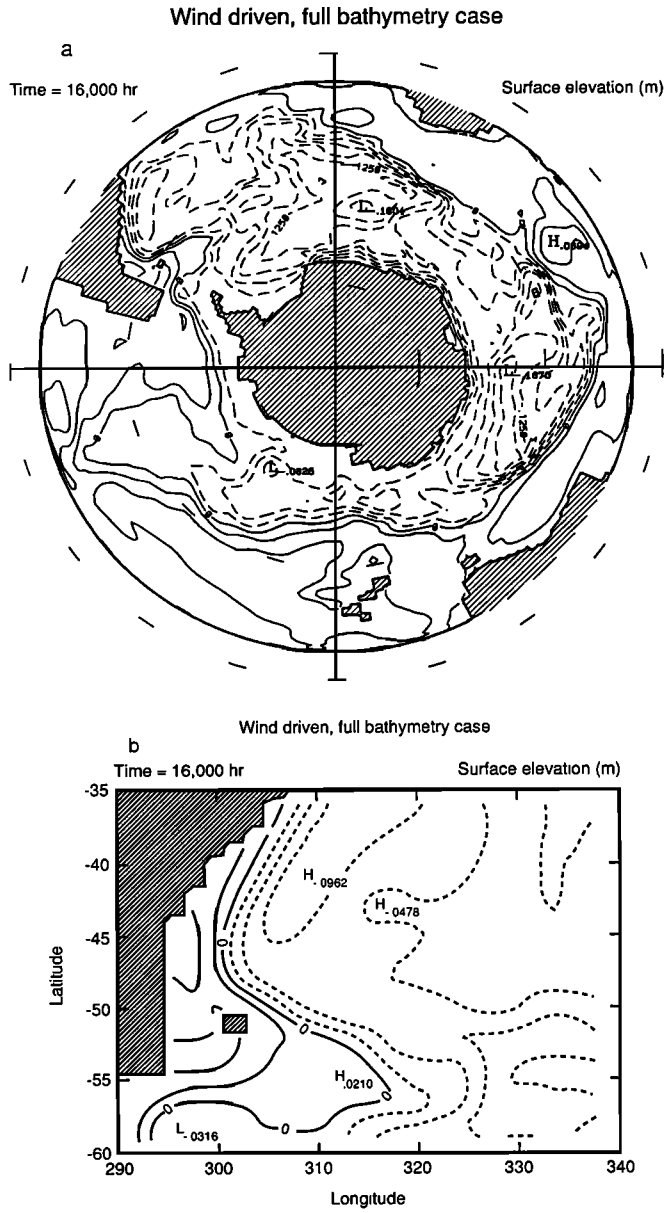

Fig. 7. Surface elevation at steady state for annual mean wind-forced Southern Ocean with full bathymetry. After 16,000 hours of simulation, the transport is 20.5 × 10^6 m^3 s^{-1}. Surface elevation (in meters) is indicated by thin lines; negative contour lines are dashed. Heavy lines indicate land boundaries. (*a*) Surface elevation over the whole model domain, with a contour interval of 0.025 m. (*b*) Surface topography in the southwestern South Atlantic, with a contour interval of 0.025 m.

Internal Pressure Gradient and Wind Driven, Full Bathymetry Simulation

The steady circulation produced by the pressure force due to internal density gradients and the surface wind stress is only slightly different from the case driven only by the internal pressure gradients. The transport is 279 × 10^6 m^3 s^{-1}, which is very close to the sum of the transport for the wind-driven case and the density gradient driven case. The surface elevation (Figure 9*a*) is similar to that obtained in the previous case. Likewise, the surface topography in the southwestern South Atlantic (Figure 9*b*) is almost the same.

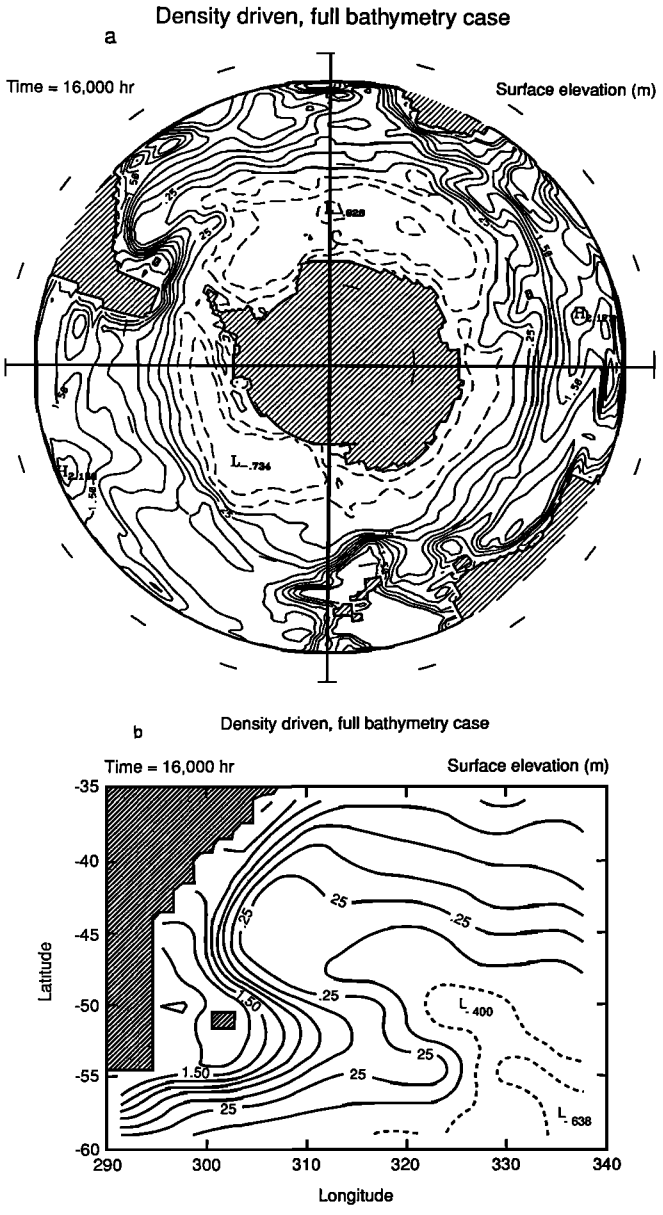

Fig. 8. Surface elevation at steady state for density-forced Southern Ocean with full bathymetry. After 16,000 hours of simulation, the transport is 256 × 10^6 m^3 s^{-1}. Surface topography (in meters) is indicated by thin lines; negative contour lines are dashed. Heavy lines indicate land boundaries. (*a*) Surface elevation over the whole model domain, with a contour interval of 0.25 m. (*b*) Surface topography in the southwestern South Atlantic, with a contour interval of 0.25 m.

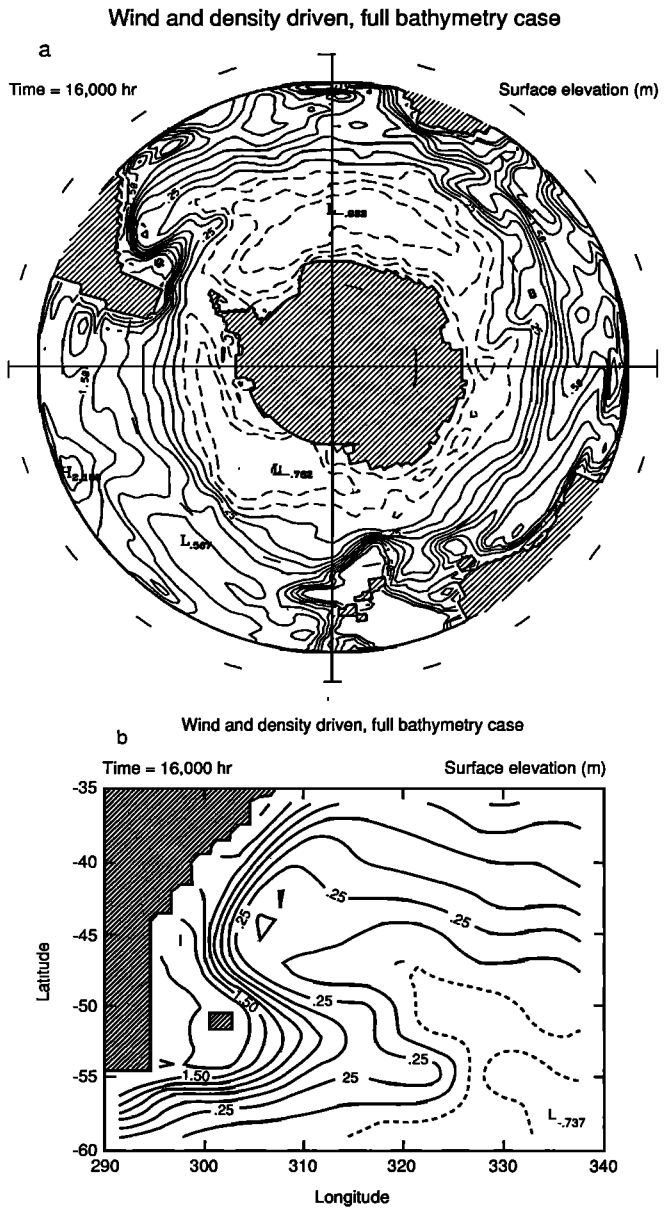

Fig. 9. Surface elevation at steady state for density- and wind-forced Southern Ocean with full bathymetry. After 16,000 hours of simulation, the transport is 279 × 10^6 m^3 s^{-1}. Surface topography (in meters) is indicated by thin lines; negative contour lines are dashed. Heavy lines indicate land boundaries. (*a*) Surface elevation over the whole model domain, with a contour interval of 0.25 m. (*b*) Surface topography in the southwestern South Atlantic, with a contour interval of 0.25 m.

Zonal Momentum Balance

The zonal momentum balance for the Southern Ocean where latitude lines are not blocked by continental boundaries, is different from that for closed ocean gyres. The momentum balance for the Southern Ocean is obtained by integrating the eastward momentum equation (1) along an unblocked latitude line. The integral of one of the nonlinear terms ($\partial u^2/\partial x$) vanishes because the eastward component of velocity u must be continuous. The remaining terms are

$$\frac{1}{L_x}\left[\int_0^{L_x} h\,\frac{\partial u}{\partial t}\,dx + \int_0^{L_x} \frac{\partial}{\partial y}(huv)\,dx - f\int_0^{L_x} hv\,dx + g\int_0^{L_x} h\,\frac{\partial \eta}{\partial x}\,dx - \int_0^{L_x} \frac{\tau^x}{\rho_0}\,dx + r\int_0^{L_x} uh\,dx + A\int_0^{L_x} \frac{\partial h}{\partial x}\,\frac{\partial u}{\partial x}\,dx - A\int_0^{L_x} h\,\frac{\partial^2 u}{\partial y^2}\,dx\right] = 0, \qquad (6)$$

where one integration by parts has been performed on the normal stress term. The terms in (6) are time change,

advection, Ekman, form drag, surface stress (or body force which represents pressure forcing due to density variations), bottom drag, normal stress, and tangential stress. At steady state, the time change and Ekman (due to conservation of mass) terms vanish. The indicated integrals (6) were evaluated along unblocked latitude lines using the simulated steady circulations from the five cases discussed in the previous section. For all of these cases, the time change, advection, Ekman, and normal stress terms are negligible and are not shown.

The zonal momentum balance for the flat bottom simulation shows that the major interaction is between wind stress and bottom stress (Figure 10*a*). Form drag is identically zero, and tangential stress is small. The major balance in this circulation is between surface stress and bottom stress, although there is a small amount of lateral diffusion of momentum into the adjacent subtropical gyres (north of 55°S).

The partial bathymetry case is represented by a three-term balance among surface stress, form drag, and bottom stress (Figure 10*b*). A majority of the balance is between surface stress and form drag, but the bottom loss accounts for about 25% of the dynamical balance. In spite of the moderately high value for the bottom and lateral friction coefficients and the strongly reduced bathymetry, the major drag mechanism is form drag due to the variable bottom.

The full bathymetry case driven by wind stress (Figure 10*c*) shows a balance similar to the reduced bathymetry case: the form drag opposes the wind stress. However, in this case, bottom drag makes only a small contribution to the overall momentum budget. Again, even though the friction coefficients are rather high, the integrated balance is primarily between wind stress and form drag.

Finally, the case driven by internal pressure gradients (Figure 10*d*; note that the momentum scale has changed) has a two-part balance between the integrated pressure gradient force and form drag with a very small contribution due to bottom friction. Tangential stress plays a negligible role in the momentum balance. If wind stress is added to the pressure gradient forcing, then the balance is identical (Figure 10*e*) with slight increases in the magnitude of the forcing and the form drag, but otherwise there is no difference.

4. Discussion

Bottom Form Drag

The difference in the wind-driven circulation between the flat bottom case and the full bathymetry case is remarkable (although well known), in that the pressure force of the bottom on the flow has the effect of reducing the circulation by a factor of 100 or more. The influence of the bathymetry is so strong that even a gentle bottom slope (15% of the true value) reduces the flow speed to within a factor of 2 of the observed value.

The problem remains that the form drag is too strong in barotropic simulations with the correct bathymetry. Typically, arguments are made that it is the bottom flow, which is smaller than the vertically averaged flow, that is responsible for the form drag, so the bathymetry can be reduced by some factor to properly scale the effect of the bottom slope [*Pedlosky*, 1987, p. 261]. However, this reduction of bathymetry simply creates another poorly known parameter which must be estimated somehow. A "correct" value is not possible, since the bathymetry also affects the path of the ACC; if the reduction parameter is chosen to give a transport of about 100×10^6 m^3 s^{-1}, then the path of the ACC is deflected too much. If the reduction parameter is chosen to give a reasonable path for the ACC, the transport is larger than the measured value. The simulation presented here with 15% bathymetry follows the latter condition that the path of the ACC is approximately correct; however, the transport is 2 times the observed value.

Internal Density Gradient Effects

At first it seems curious that the density gradients produce a force that accelerates the ACC, a result obtained earlier by *Gill and Bryan* [1971]. However, this force is a necessary mechanism for producing a realistic simulation of the Southern Ocean. The dynamically consistent way to provide for the influence of the internal density structure is to integrate a three-dimensional model. However, an alternative to this is to estimate the vertically integrated effect of the density structure and include it as a body force. The drawback of this method is that the density, which has been estimated from time aliased observations and has been spatially smoothed to some extent, is not modified by the circulation, which reacts to bathymetry as well as density gradients, to produce an appropriate geostrophic balance.

It is clear from the general structure of the simulation (Figure 8*a*) that the pressure force due to the internal density gradients is of the proper sign and magnitude to provide a more realistic transport in the presence of bathymetry than is produced by wind forcing alone. In summary, the integrated density gradients provide the proper pressure gradient force to allow the flow to negotiate the various ridges in the Southern Ocean.

Eddy Effects

Several recent modeling studies have investigated the effects of mesoscale eddies on the dynamics of flow in a zonal channel [*Wolff and Olbers*, 1989; *Treguier and McWilliams*, 1990; *Wolff et al.*, 1991]. These studies focus on the process of momentum transport by eddies and consider, in particular, how standing eddies (permanent distortions of the density surfaces) produce a downward transmission of momentum. The ultimate sink for momentum in these models is form drag (mainly) and bottom friction.

The cases considered here lead to conclusions similar to those of *Wolff et al.* [1991] on the retarding influence of bathymetry. The integrated momentum balance discussed here compares most closely with the vertically and zonally integrated momentum balance for flow over topography which extends across the channel [*Wolff et al.*, 1991, case BR, Figure 12]. The major balance in both cases is between surface forcing and form drag. Their simulation includes the influence of standing and transient eddies which are not present in the one-layer simulations considered here. Nevertheless, the results of these two sets of experiments agree despite the difference in the complexity of the models being used.

5. Summary

The simulations presented here confirm the previously proposed hypothesis [*Munk and Palmén*, 1951] for the ACC

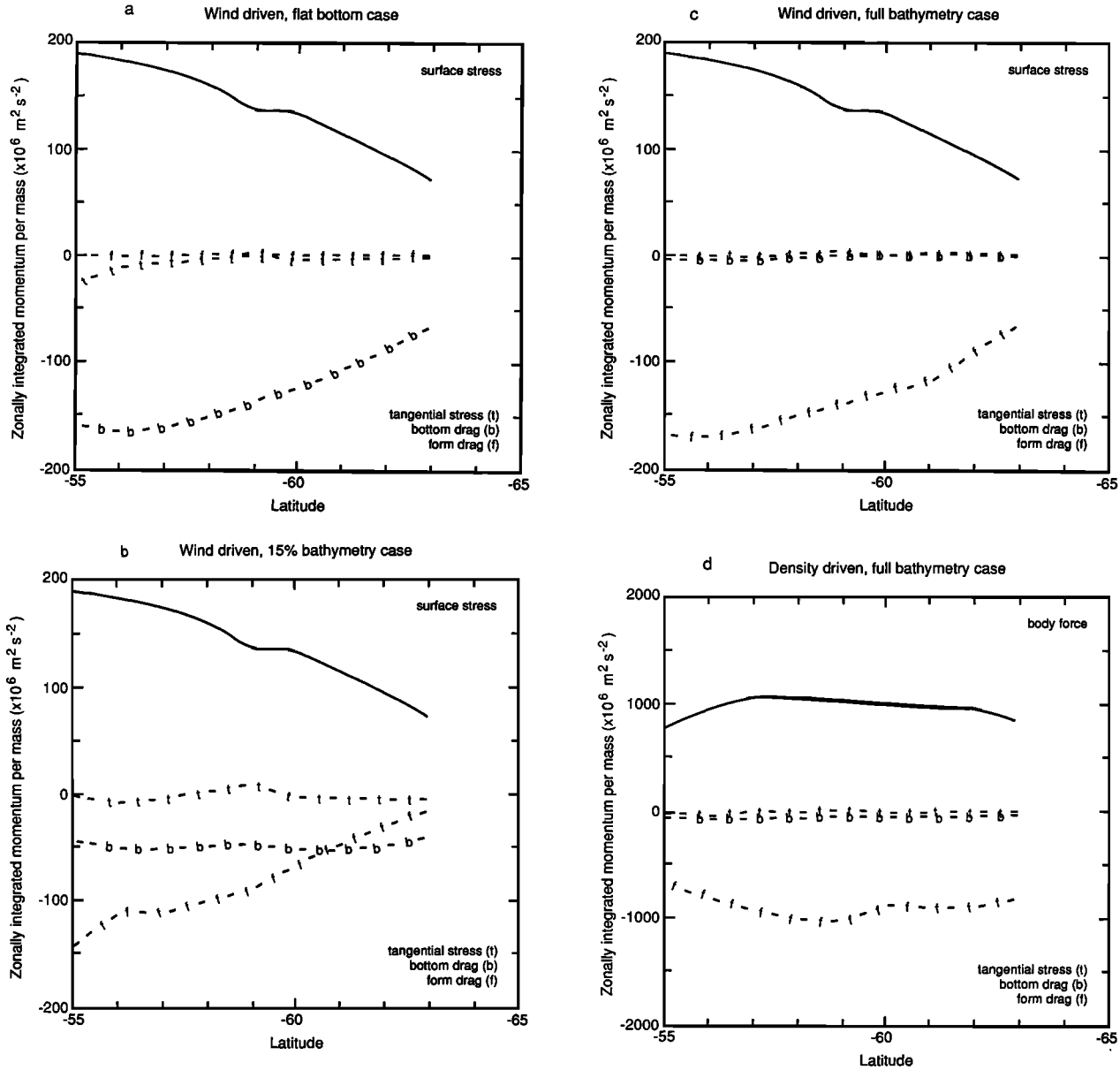

Fig. 10. The depth-integrated, zonally averaged momentum per unit mass ($\times 10^{-6}$ m^2 s^{-2}) as a function of latitude for the five cases after 16,000 hours of simulation. The solid line is wind stress (or body force per unit depth due to density gradients), and dashed lines are tangential (lateral) stress, bottom drag, and form drag (formulas are given in the text). Each of the dashed lines is identified by a letter t, b, or f to indicate tangential, bottom, or form drag. (*a*) Wind-forced, flat bottom case. (*b*) Wind-forced case with bathymetry reduced to 15% of the true value. (*c*) Wind-forced case with full bathymetry. (*d*) Density-forced case with full bathymetry. (*e*) Density- and wind-forced case with full bathymetry.

that form drag is effective in balancing the force due to the surface wind stress. In fact, this effect is so strong that bathymetry with only 15% of the true amplitude reduces the transport of the ACC from over 500 $\times$ 10^6 m^3 s^{-1} to about 180 $\times$ 10^6 m^3 s^{-1}. If the true bathymetry is used, the total transport is reduced to an unrealistic value of about 20 $\times$ 10^6 m^3 s^{-1}. Analysis of the zonally integrated momentum in the unblocked part of the Southern Ocean shows that the bottom drag balances the surface forcing, even for simulations that use viscous coefficients that are in the upper range of acceptable values.

The effect of the climatological density structure on the

Fig. 10. (continued)

vertically integrated circulation in the Southern Ocean is to accelerate the flow, as was first discussed by *Gill and Bryan* [1971]. This earlier simulation had insufficient drag, since the bathymetry was everywhere flat except in Drake Passage, where a partial vertical wall was included to mimic blocking. In the present study, the coupled effect of stratification and form drag from finite width bathymetry produces a more realistic circulation.

In contrast to mid-latitude gyres [*Anderson and Killworth*, 1977], where the steady wind-driven circulation is insulated from the effect of bathymetry by stratification, the density variation is required in the Southern Ocean in order to produce a realistic simulation of the ACC. The observed density structure is such that the pressure gradient force pushes the flow across bathymetry that would, in the absence of the density field, block the circulation. However, the processes that produce the observed density structure of the Southern Ocean are not clear. One possibility is that the observed surface wind stress would force an initially still and vertically stratified Southern Ocean into the observed state. Alternatively, the surface heat flux may be required to produce the observed density distribution. The answer to this question requires the analysis of more comprehensive models.

Acknowledgments. Tim Boyer is thanked for help with the calculation of the force due to the internal density gradients. This research was supported by the National Science Foundation under grant OCE-8996235.

REFERENCES

Anderson, D. L. T., and P. D. Killworth, Spin-up of a stratified ocean, with topography, *Deep Sea Res.*, *24*, 709–732, 1977.

Bryan, K., and M. D. Cox, The circulation of the World Ocean: A numerical study, Part I, A homogeneous model, *J. Phys. Oceanogr.*, *2*, 319–335, 1972.

Clarke, A. J., The dynamics of large-scale, wind-driven variations in the Antarctic Circumpolar Current, *J. Phys. Oceanogr.*, *12*, 1092–1105, 1982.

Gill, A. E., *Atmosphere-Ocean Dynamics*, 662 pp., Academic, San Diego, Calif., 1982.

Gill, A. E., and K. Bryan, Effects of geometry on the circulation of a three-dimensional southern hemisphere ocean model, *Deep Sea Res.*, *18*, 685–721, 1971.

Gordon, A. L., and T. N. Baker, *Southern Ocean Atlas*, 31 pp., Amerind, New Delhi, 1986.

Gordon, A. L., E. Molinelli, and T. Baker, Large-scale relative dynamic topography of the Southern Ocean, *J. Geophys. Res.*, *83*, 3023–3032, 1978.

Hidaka, K., and M. Tsuchiya, On the Antarctic Circumpolar Current, *J. Mar. Res.*, *12*, 214–222, 1953.

Inoue, M., Modal decomposition of low-frequency currents and baroclinic instability at Drake Passage, *J. Phys. Oceanogr.*, *15*, 1157–1181, 1985.

Johnson, G. C., and H. L. Bryden, On the size of the Antarctic Circumpolar Current, *Deep Sea Res.*, *36*, 39–53, 1989.

Johnson, J. A., and R. B. Hill, A three-dimensional model of the Southern Ocean with bottom topography, *Deep Sea Res.*, *22*, 745–751, 1975.

Klinck, J. M., Vorticity dynamics of seasonal variations of the Antarctic Circumpolar Current from a modelling study, *J. Phys. Oceanogr.*, *21*, 1515–1533, 1991.

Leendertse, J. J., Aspects of a computational model for long period water-wave propagation, *Memo. RM-5294-PR*, 165 pp., Rand Corp., Santa Monica, Calif., 1967.

McWilliams, J. C., W. R. Holland, and J. H. S. Chow, A description of numerical Antarctic circumpolar currents, *Dyn. Atmos. Oceans*, *2*, 213–291, 1978.

Mesinger, F., and A. Arakawa, Numerical methods used in atmospheric models, vol. I, *GARP Publ. Ser.*, *17*, 65 pp., 1976.

Munk, W. H., and E. Palmén, Note on the dynamics of the Antarctic Circumpolar Current, *Tellus*, *3*, 53–56, 1951.

Nowlin, W. D., Jr., and J. M. Klinck, The physics of the Antarctic Circumpolar Current, *Rev. Geophys.*, *24*, 469–491, 1986.

Pedlosky, J., *Geophysical Fluid Dynamics*, 2nd ed., 710 pp., Springer-Verlag, New York, 1987.

Peterson, R. G., and T. Whitworth, III, The subantarctic and polar fronts in relation to deep water masses through the southwestern Atlantic, *J. Geophys. Res.*, *94*, 10,817–10,838, 1989.

Schulman, E. E., A study of topographic effects, in *Numerical Models of Ocean Circulation*, pp. 147–167, National Academy of Sciences, Washington, D. C., 1975.

Semtner, A. J., Jr., and R. M. Chervin, A simulation of the global ocean circulation with resolved eddies, *J. Geophys. Res.*, *93*, 15,502–15,522, 1988.

Treguier, A. M., and J. C. McWilliams, Topographic influences on wind-driven, stratified flow in a β-plane channel: An idealized model for the Antarctic Circumpolar Current, *J. Phys. Oceanogr.*, *20*, 321–343, 1990.

Trenberth, K. E., J. G. Olson, and W. G. Large, A global ocean wind stress climatology based on ECMWF analyses, Natl. Cent. for Atmos. Res., *Rep. NCAR/TN-338+STR*, 93 pp., Boulder, Colo., 1989.

Whitworth, T., III, Monitoring the transport of the Antarctic Circumpolar Current at Drake Passage, *J. Phys. Oceanogr.*, *13*, 2045–2057, 1983.

Whitworth, T., III, and R. G. Peterson, Volume transport of the Antarctic Circumpolar Current from bottom pressure measurements, *J. Phys. Oceanogr.*, *15*, 810–816, 1985.

Wolff, J.-O., and D. J. Olbers, The dynamical balance of the Antarctic Circumpolar Current studied with an eddy-resolving quasigeostrophic model, in *Mesoscale/Synoptic Coherent Structures in Geophysical Turbulence*, *Oceanogr. Ser. 50*, edited by J. C. J. Nihoul, pp. 435–458, Elsevier, New York, 1989.

Wolff, J.-O., E. Maier-Reimer, and D. J. Olbers, Wind-driven flow over topography in a zonal β-plane channel: A quasi-geostrophic model of the Antarctic Circumpolar Current, *J. Phys. Oceanogr.*, *21*, 236–264, 1991.

J. M. Klinck, Department of Oceanography, Old Dominion University, Norfolk, VA 23529.

(Received June 28, 1991;
revised May 11, 1992;
accepted August 19, 1992.)